In situ Characterization of SiO_2 Nanoparticle Biointeractions Using BrightSilica

*Daniela Drescher, Ingrid Zeise, Heike Traub, Peter Guttmann, Stephan Seifert, Tina Büchner, Norbert Jakubowski, Gerd Schneider, and Janina Kneipp**

By adding a gold core to silica nanoparticles (BrightSilica), silica-like nanoparticles are generated that, unlike unmodified silica nanoparticles, provide three types of complementary information to investigate the silica nano-biointeraction inside eukaryotic cells in situ. Firstly, organic molecules in proximity of and penetrating into the silica shell in live cells are monitored by surface-enhanced Raman scattering (SERS). The SERS data show interaction of the hybrid silica particles with tyrosine, cysteine and phenylalanine side chains of adsorbed proteins. Composition of the biomolecular corona of BrightSilica nanoparticles differs in fibroblast and macrophage cells. Secondly, quantification of the BrightSilica nanoparticles using laser ablation inductively coupled plasma mass spectrometry (LA-ICP-MS) micromapping indicates a different interaction of silica nanoparticles compared to gold nanoparticles under the same experimental conditions. Thirdly, the metal cores allow the investigation of particle distribution and interaction in the cellular ultrastructure by cryo nanoscale X-ray tomography (cryo-XT). In 3D reconstructions the assumption is confirmed that BrightSilica nanoparticles enter cells by an endocytotic mechanism. The high SERS intensities are explained by the beneficial plasmonic properties due to agglomeration of BrightSilica. The results have implications for the development of multi-modal qualitative and quantitative characterization in comparative nanotoxicology and bionanotechnology.

1. Introduction

Silica nanoparticles, similar to other nanomaterials can be taken up by animal cells. Meanwhile, the uptake of silica nanoparticles by biological cells has been studied and utilized in many applications of imaging and therapeutics.[1] In order to understand and suppress potential nanotoxic action[2] and optimize drug delivery tools,[3] it is crucial to elucidate the interaction of the silica nanoparticles with the cellular biomolecules. Aside from other parameters such as size, shape, agglomeration,[4] and temperature[5] the molecules interacting with the nanoparticle surfaces critically determine their uptake and processing by the cells.[6] The composition of the protein biomolecular corona of silica nanoparticles has been determined in in vitro systems, such as solutions of plasma proteins,[7] and also after recovering of extracellular nanoparticles from cultured cells.[6a]

Nanoparticles with silica surface, specifically gold core@silica shell structures have been shown to be taken up by animal cells using Raman scattering experiments.[8] In previous work, the SERS signals from the reporter molecules 4-mercaptobenzoic acid,[8a,b] DTNB[8c] or from dyes[8d,e] incorporated in the silica shell were observed and mapped in cultured cells. Information about the biomolecular surroundings of the silica nanoparticles is not accessible in the experiments that were reported so far.

In previous studies, we have investigated the corona composition of plasmonic nanoparticles in vivo and related the results to the nanoparticle interaction with the cellular ultrastructure, showing that a combination of surface-enhanced Raman scattering (SERS) with ultrastructural studies,[9] specifically with synchrotron based cryo X-ray tomography (cryo-XT) is very useful.[10] As reported recently, quantification of such nanoparticles can be achieved with high spatial resolution by using laser ablation inductively coupled plasma mass spectrometry (LA-ICP-MS) micromapping.[11]

In this study, we have utilized silica nanoparticles with a plasmonic core, termed BrightSilica, which allow for the combination of SERS, cryo-XT, and LA-ICP-MS, and thus give a comprehensive view on the interaction of silica nanoparticles with live cells at the molecular level. BrightSilica with gold and silver core were studied regarding cellular uptake and processing in two cell lines, 3T3 fibroblast cells and J774 macrophages. As reported in the following, cryo nanoscale X-ray tomography using synchrotron radiation[12] allows not only the visualization of the cellular ultrastructure with a 3D resolution,[10,13] but also

D. Drescher, I. Zeise, S. Seifert, T. Büchner, Prof. J. Kneipp
Humboldt-Universität zu Berlin
Department of Chemistry
Brook-Taylor-Str. 2
12489, Berlin, Germany
E-mail: janina.kneipp@chemie.hu-berlin.de
D. Drescher, Dr. H. Traub, S. Seifert, T. Büchner, Dr. N. Jakubowski, Prof. J. Kneipp
BAM Federal Institute for Materials Research and Testing
Richard-Willstätter-Str. 11, 12489 Berlin, Germany
Dr. P. Guttmann, Dr. G. Schneider
Helmholtz-Zentrum Berlin für Materialien und Energie
Institute for Soft Matter and Functional Materials
Albert-Einstein-Str. 15, 12489 Berlin, Germany

DOI: 10.1002/adfm.201304126

the observation of the BrightSilica nanoparticles. While the surface of the nanoparticles is a silica surface, the core can be used to monitor molecules of the nanoparticle corona that interact with the silica surface and those interacting with the silica subsurface using their SERS spectra. This in situ molecular characterization is possible because the molecules at the sub-surface of the nanoparticles are in the local field of the plasmonic (gold) core. As will be demonstrated, the intense signals from the biomolecules at the silica surface can also be attributed to the penetration of surrounding biomolecules into the silica material. Quantitative uptake and distribution of nanoparticles with a silica surface obtained by LA-ICP-MS micromapping will be compared with those of uncoated nanoparticles.

2. Results and Discussion

2.1. Characterization of 'BrightSilica' Nanoparticles

To study the nano-biointeraction of silica nanoparticles, we prepared silica nanoparticles with gold and silver cores by growing silica shells of varying thickness around gold and silver nanoparticles. Size and morphology of the nanoparticles were characterized by transmission electron microscopy (TEM) (**Figure 1**) and dynamic light scattering (Figure S1).

Both gold and silver cores display high homogeneity in size (Figure 1A,D) and were covered with a shell of 1-2 nm (Figure 1B,C) and 2–4 nm thickness (Figure 1E,F), respectively and are termed BrightSilica(Au) and BrightSilica(Ag) in the following. Their diameters of 31 ± 5 nm (BrightSilica(Au)) and 57 ± 20 nm (BrightSilica(Ag)) are mainly determined by the diameters of the cores. The presence of the plasmonic cores in BrightSilica(Au) and BrightSilica(Ag) is clearly evidenced by the absorbance spectra, displaying maxima typical of the gold and silver cores (for examples see Figure S2).

As we aimed at the delivery of BrightSilica nanoparticles into live cells, the particle stability under incubation conditions, which plays a crucial role for the cellular uptake efficiency regarding aggregation and aggregate size[4c,6a,14] was determined. BrightSilica nanoparticles were suspended in cell culture medium (DMEM and 10% FCS), incubated for 24 h and investigated by dynamic light scattering (Figure S1). The results are compared with uncoated gold and silver nanoparticles. All nanoparticles are stable in the culture medium containing 10% fetal calf serum, and display a slight increase of their hydrodynamic diameter, indicating the adsorption of a biomolecular corona[7] (Figure S1).

Both BrightSilica(Ag) and BrightSilica(Au) show SERS enhancement factors in the range of 10^2 and 10^3 (for example spectra see Figure S3B). The enhancement factors were determined using the dye crystal violet and are in accordance with previous experimental[15] and theoretical[16] findings on SERS enhancement by individual gold and silver nanoparticles. From the experiments with crystal violet we conclude that the local field of the plasmonic core enables SERS of the molecule. Therefore, BrightSilica nanoparticles can be utilized to investigate the molecules in their proximity, that is, the biomolecules constituting the nanoparticle corona and those interacting with the sub-surface of the silica coating.

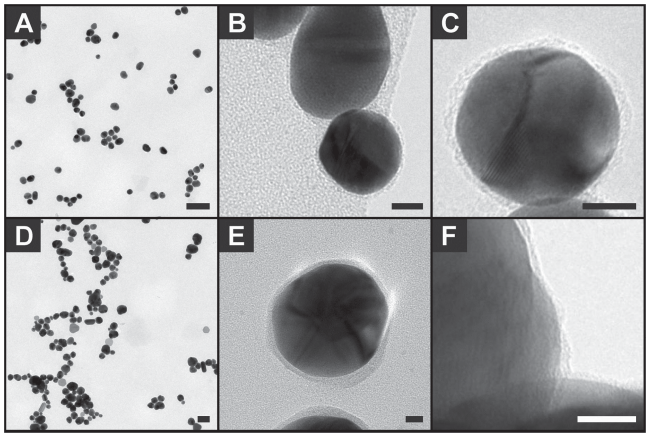

Figure 1. Transmission electron micrographs of BrightSilica(Au) (A–C), BrightSilica(Ag) (D–F). Thicknesses of the silica layers in the displayed samples were determined to be (A,B) 1.4 ± 0.3 nm, (C) 1.7 ± 0.4 nm, (D,F) 1.7 ± 0.5 nm and (E) 3.7 ± 1.4 nm. Scale bars represent 100 nm (A,D) and 10 nm (B–F).

2.2. Metal Nanoparticles with Silica Shells Can Be Detected and Imaged in Cells with Cryo Nanoscale X-ray Tomography

To assess general aspects regarding the detection of silica nanoparticles and silica-coated metal nanoparticles by cryo X-ray tomography (cryo-XT), silver nanoparticles were also covered with silica shells of greater thickness, e.g. 49 ± 4 nm or 29 ± 5 nm (for TEM images see Figure S4). They are termed SiO_2(49 nm)@Ag and SiO_2(29 nm)@Ag, respectively. Since the local field extends only a few nanometers from the plasmonic core, no SERS signals are expected for nanoparticles surrounded by thicker silica shells. Thus, for optical mapping, they were further complemented by encapsulated *para*-aminothiophenol (*p*ATP) as reporter molecule providing a characteristic SERS spectrum[17] (Figure S3). Thickness and homogeneity of the silica coating of these nanoparticles were verified by scanning transmission electron microscopy – energy dispersive X-ray spectroscopy (STEM-EDX, Figure S5) and energy-filtered transmission electron microscopy (EFTEM, Figure S6).

To verify the intracellular uptake and gain information about the spatial distribution of nanoparticles with respect to cellular substructures, ultrastructural information was obtained from cryo-XT using synchrotron radiation (**Figure 2**, **Figure 3**). This technique allows the visualization of the 3-dimensional assembly of nanoparticles in whole vitrified eukaryotic cells with a thickness of up to 10 µm at nanoscale resolution (36 nm).[10,13] Employing a photon energy of 510 eV, the contrast of organic material or metal nanoparticles is higher than that of vitreous ice due to the stronger absorption of soft X-rays, in the so-called X-ray water window.[12a,b,18]

In the experiment, adherent fibroblast cells and macrophages were exposed to SiO_2(29 nm)@Ag (Figure 2A,B) and SiO_2(49 nm)@Ag nanoparticles (Figure 2C–E, Figure 3), respectively, for 24 h under standard cell culture conditions. Owing to the high linear absorption coefficient of silver (20.7 μm^{-1}), the metal cores appear dark in Figure 2 and highlight the core-shell

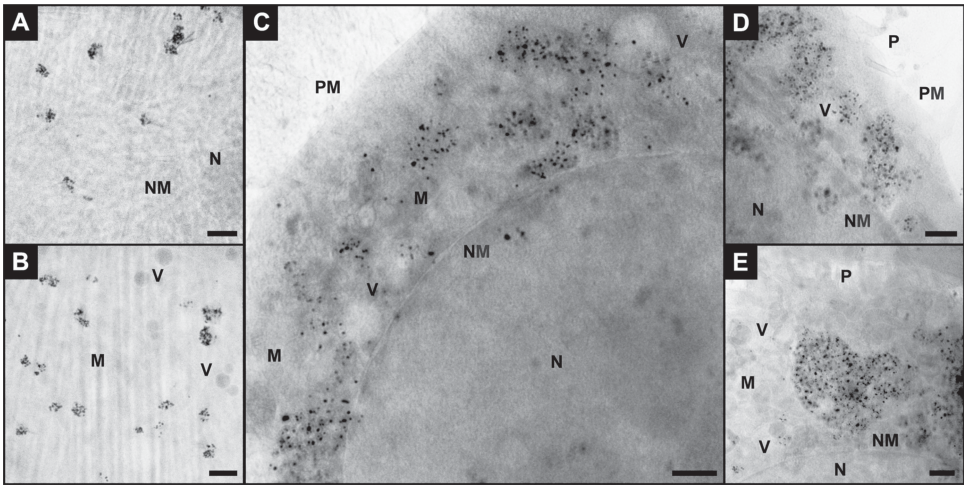

Figure 2. Nanoscale X-ray microscopic imaging of vitrified 3T3 fibroblast cells after incubation with SiO_2(29 nm)@Ag (A,B) and J774 macrophages after exposure to SiO_2(49 nm)@Ag (C–E) for 24 h. The metal cores appear dark, the surrounding silica layers can be discriminated. All images were acquired with a 25 nm zone plate (9.8 nm pixel size). Scale bars: 1 µm. Abbreviations: N, nucleus; NM, nuclear membrane; M, mitochondrion; V, vesicle; PM, plasma membrane; P, pseudopod.

nanoparticles inside the cells. Despite the small differences in absorption contrast of silica and organic matter, the silica coating itself is also visible in the biological matrix. The persistence of the silica layers under physiological conditions is clearly revealed from the X-ray tomography data (Figure 3A–D). Large quantities of the silica-coated silver nanoparticles were observed in the cellular interior of both, fibroblast and macrophage cells as aggregates that differ in size and shape, and no particles were found inside the cell nuclei. In macrophages (Figure 2C–E, Figure 3), particles are also enclosed in endolysosomal vesicles in addition to a phagosomal localization, indicative of both endocytosis and phagocytosis as uptake mechanisms. Aggregates consisting of 5 to 50 nanoparticles are found inside cell vesicles in the proximity of the nuclear membrane and other cellular compartments, e.g., of mitochondria. The organization of the core-shell nanoparticles in the 3D architecture of the macrophages is visualized in the tomographic reconstruction of Figure 3 and in the Movie S1 in the Supporting Information.

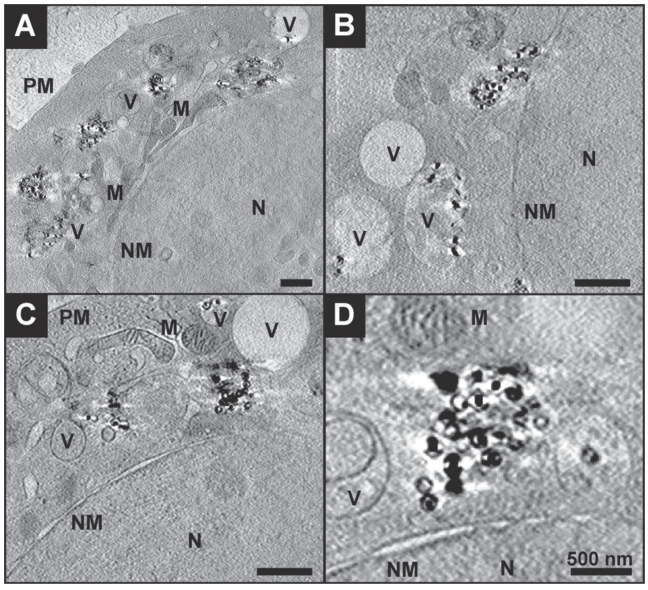

Figure 3. Slices of a tomographic reconstruction of a vitrified J774 macrophage cell after incubation with SiO_2(49 nm)@Ag nanoparticles in cell culture medium for 24 h. The particles are enclosed in vesicular structures in the proximity of mitochondria or the cell nucleus. All images were acquired with a 25 nm zone plate (9.8 nm pixel size). A pixel binning of 2 × 2 was used. Scale bars: 1 µm. Abbreviations: N, nucleus; NM, nuclear membrane; M, mitochondrion; V, vesicle; PM, plasma membrane.

The particle size distribution in the incubation medium (Figure S1E) proves the presence of primary particles and/or very small aggregates before endocytotic or phagocytotic uptake. Therefore, the formation of the larger nanoparticle aggregates observed in the cryo-XT data must occur during uptake or intracellular processing. X-ray microscopic images also show individual nanoparticles as well as small aggregates in endocytotic vesicles in the cytoplasm after 24 h of incubation. The data indicate that silica nanoparticles larger than 100 nm in diameter can be efficiently taken up and processed by both, macrophages and fibroblast cells, in agreement with the results of transmission electron microscopic studies.[19]

Silica-coated gold and silver nanoparticles with shell thickness of many nanometers can be used as SERS labels in live cells when a reporter molecule is encapsulated. When fibroblast and macrophage cells were exposed to SiO_2(29 nm)@Ag nanoparticles, Raman maps (Figure S7) were obtained that clearly reveal the presence of the encapsulated reporter molecules. Figure S7 shows bright field images and representative SERS maps using the spectral signature of *p*ATP (see also Figure S3A) that suggest the uptake of SiO_2(29 nm)@Ag particles into 3T3 fibroblast and J774 macrophage cells. It should be noted that the SiO_2(29 nm)@Ag nanoparticles were used in these experiments mainly to evaluate X-ray microscopic imaging and quantification by LA-ICP-MS (see below) of silica-coated nanoparticles. In the SERS experiments, such nanoparticles with relatively thick silica layers always need to

carry a reporter molecule in order to be identified, and hence provide the function of a label. The aim of this work here is to obtain intrinsic information from the nm-scaled environment and of the silica surface inside the cells. As discussed above, plasmonic nanostructures with silica layers of only very few nanometer thickness, that is, BrightSilica nanoparticles, have to be applied. In this way, the 3D information about nanoparticle distribution in cellular substructures from cryo-XT will be combined with the molecular information on BrightSilica nanoparticle sub-surface composition by SERS.

2.3. Uptake of BrightSilica Nanoparticles

The interaction of nanoparticles with cells, regarding the mechanism and efficiency of cellular uptake, is determined by the physico-chemical properties of the nanomaterial, e.g., size, shape, and surface modification.[20] Coating of silver or gold nanoparticles even with thin layers of silica changes the surface termination of the particles that is expected to result in differences in the intracellular distribution and quantity. To evaluate the influence of the cell type and nanoparticle surface modification on the number of nanoparticles taken up by the cells, laser ablation inductively coupled plasma mass spectrometry (LA-ICP-MS) micromapping experiments were conducted on individual fibroblast cells and macrophages. In these experiments, the uptake of BrightSilica(Ag) is compared with that of SiO_2(29 nm)@Ag and with uncoated silver nanoparticles (**Figure 4**), as well as that of BrightSilica(Au) with uncoated gold nanoparticles (Figure S8). Whereas silica itself would not be suitable for high-resolution LA-ICP-MS imaging because of the low sensitivity and high background signal, the potential of this method for the quantification of gold and silver nanoparticles was recently demonstrated.[11] The metal core of the BrightSilica nanoparticles enables sensitive LA-ICP-MS analysis of the particle uptake into eukaryotic cells with high spatial resolution with respect to their intracellular localization and quantification.

Figure 4 displays the distribution of silica-like nanoparticles as an overlay of the color encoded $^{107}Ag^+$ local intensity map with the corresponding bright field micrograph of fibroblast cells (Figure 4A–C) and macrophages (Figure 4D–F). The 2D intensity maps of the fibroblast cells show a similar distribution of uncoated silver nanoparticles (Figure 4A) and BrightSilica(Ag) (Figure 4B) and are comparable to citrate-stabilized silver nanoparticles in 3T3 fibroblast cells reported before.[11] After 24 hours of incubation, the particles are localized in the cytosol with spots of high $^{107}Ag^+$ intensity in the proximity of the cell nucleus, which suggests the accumulation of particle aggregates in this region. The low signal intensity in the region of cell nuclei can be explained by nanoparticles localized in the small volume above or below the nucleus. Nanoparticles with thicker shells SiO_2(29 nm)@Ag provide the possibility to compare uptake of relatively large silica-like nanoparticles with smaller ones (BrightSilica with thin shells) at an *identical* size of the plasmonic cores. The incubation of SiO_2(29 nm)@Ag (Figure 4C) that have a size larger than 100 nm (126 ± 26 nm) leads to lower $^{107}Ag^+$ intensities and fewer high-intensity spots in the cytosol of fibroblast cells compared to the experiments with smaller nanoparticles (Figure 4A,B).

As visible in Figure 4D–F, in macrophage cells, the intensity of $^{107}Ag^+$ and thus the number of uncoated and silica-coated

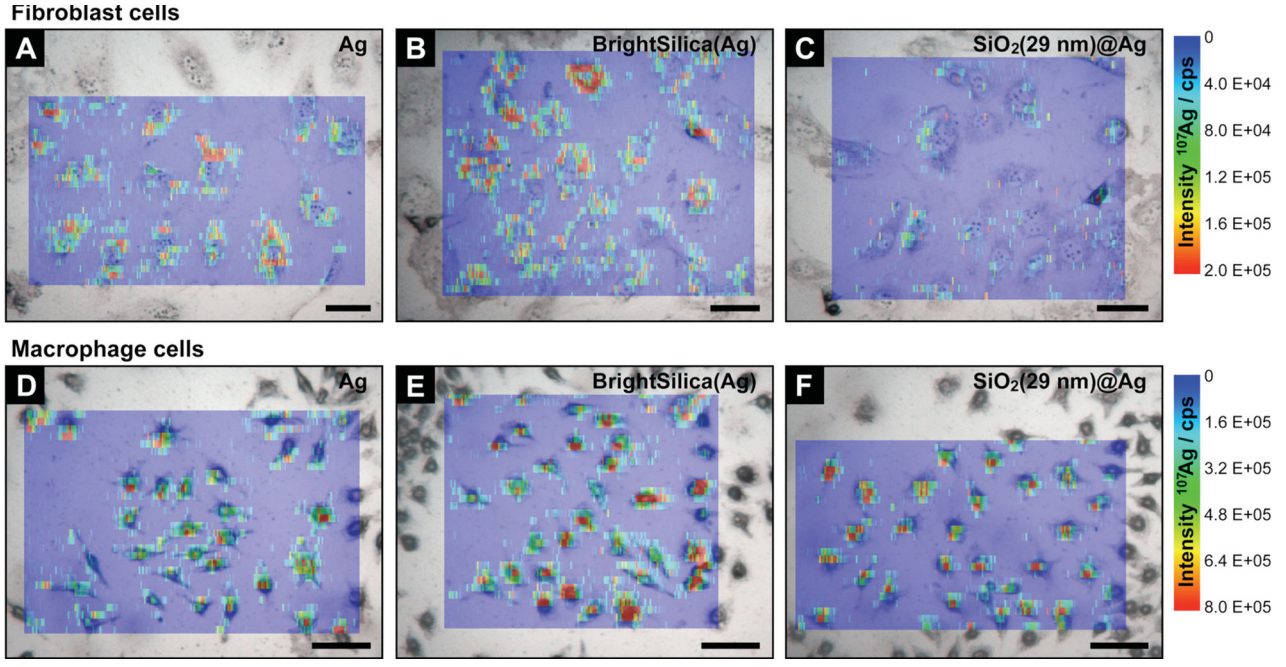

Figure 4. Bright field micrographs of fixed 3T3 fibroblast cells (A-C) and J774 macrophages (D-F) superimposed with LA-ICP-MS images of $^{107}Ag^+$ intensity distribution. Cells were incubated with uncoated and silica-coated silver nanoparticles for 24 h: Silver nanoparticles (A, D), BrightSilica(Ag) (B, E) and SiO_2(29 nm)@Ag (C, F). Scale bars represent 50 micrometers. Parameters: Laser spot size 8 µm, scan speed 8 µm/s, repetition rate 5 Hz, pixel size 1.5 × 8 µm (fibroblast cells) and 1.5 × 7 µm (macrophages), fluence 0.6 J cm^{-2} (fibroblast cells) and 4.0 J cm^{-2} (macrophages).

silver nanoparticles does not differ significantly, inspite of different surface modifications and particle sizes. In contrast to fibroblast cells, macrophages internalize the larger SiO_2(29 nm)@Ag as efficiently as the smaller BrightSilica(Ag) nanoparticles. The perinuclear region of the cells is characterized by spots with very high $^{107}Ag^+$ intensities, indicating an elevated nanoparticle concentration in late endosomes, which is visible prominently in the line scans (Figure S9) extracted from the maps (Figure 4). Depending on the particle type, the line scans show differences in the absolute intensity and density of the $^{107}Ag^+$ signals for fibroblast cells and macrophages.

The $^{197}Au^+$ distribution of BrightSilica(Au) in 3T3 fibroblast cells and J774 macrophages (Figure S8) proves very similar to that of BrightSilica(Ag) and uncoated silver nanoparticles (Figure 4) as well as gold nanoparticles.[11]

In general, the LA-ICP-MS micromapping data on the uptake and distribution of silica-coated metal nanoparticles comply with the results of cryo-XT and with results from other studies on the intracellular processing of silica nanoparticles.[4c,6a,21]

Based on the LA-ICP-MS data shown in Figure 4 and Figure S8, the relative integrated intensities of $^{107}Ag^+$ and $^{197}Au^+$, reflecting a number of nanoparticles per cell, were determined (**Figure 5**). Owing to cell-to-cell variation with respect to cell size, morphology, and uptake efficiency, the standard deviation appears relatively high. In fibroblast cells, the relative integrated intensity of $^{107}Ag^+$ and $^{197}Au^+$ differs for the different types of nanomaterials. As the cellular uptake by 3T3 fibroblasts strongly depends on the particle size, the relative integrated intensity of $^{107}Ag^+$ is about 6 times higher for BrightSilica(Ag) with a diameter of 57 nm than for the 126 nm sized SiO_2(29 nm)@Ag particles. Silica nanoparticles with a diameter smaller than 100 nm can be efficiently taken up by fibroblast cells by means of endocytosis.[4c,19c] A slight decrease in particle uptake can be noticed for the BrightSilica nanoparticles compared to the respective uncoated gold and silver nanoparticles of roughly the same size (Figure 5). For macrophages, the relative integrated intensities of $^{107}Ag^+$ and $^{197}Au^+$ are very similar upon incubation with unmodified and silica-coated metal nanoparticles. These observations demonstrate that BrightSilica as well as uncoated silica nanoparticles possess a similar uptake efficiency into macrophage and fibroblast cells as gold and silver nanoparticles of the same size and concentration.

Considering the influence of the cell type, the number of nanoparticles per cell does not differ significantly for fibroblast cells and macrophages (except for SiO_2(29 nm)@Ag) despite the differences in cell volume and uptake mechanism. However, the local particle concentration per sampled spot is much higher for macrophages than for fibroblast cells. This is in accord with their function as phagocyte in the immune system. While fibroblast cells are known to endocytose nanoparticles up to 150 nm in diameter,[4c,19c] macrophages can internalize small and large particles with up to 3 µm in size by endocytosis or phagocytosis.[14,22] For this reason, the intracellular concentration of SiO_2(29 nm)@Ag nanoparticles with a size larger than 100 nm is higher in macrophages compared to fibroblast cells under the same experimental conditions. As discussed above in the X-ray microscopic images (Figure 2), small and large nanoparticle aggregates are visible in endo-lysosomal vesicles and phagosomes of the macrophages. This is also supported by the high amount of intracellular nanoparticles detected with LA-ICP-MS.

2.4. 3D Distribution of BrightSilica Nanoparticles

X-ray microscopic imaging was performed to analyze the 3D distribution and aggregate morphology of BrightSilica nanoparticles in 3T3 fibroblast cells (**Figure 6**) and J774 macrophages (Figure S10) after 24 h of incubation. In fibroblast cells (Figure 6A–D), uncoated and BrightSilica nanoparticles in the same size range can be exclusively found in vesicular structures in the vicinity of the nuclear membrane. As visible in the X-ray microscopic tilt series (Movie S2-S5), no particles are taken up into the cell nucleus. After 24 h of incubation, individual nanoparticles as well as aggregates can be observed in the cell interior. Independent of the surface modification, the movies and the X-ray microscopic images reveal a similar 3D distribution for BrightSilica (Figure 6B,D; Movie S3 and S5) and the metal nanoparticles (Figure 6A,C; Movie S2 and S4), indicating a similar uptake behaviour of silica-coated and uncoated gold and silver nanoparticles of the same size. While in the incubation medium the particles are stabilized by steric repulsion upon the adsorption of serum proteins (Figure S1), the X-ray microscopy data provide evidence that inside the cell, particle destabilization is induced by cellular processes associated with endosomal uptake and multivesicular fusion, resulting in different sizes and morphologies of particle aggregates.

Compared to fibroblast cells, in the macrophage cells micrometer-sized particle aggregates containing more than 100 nanoparticles can be observed (Figure S10). Particle

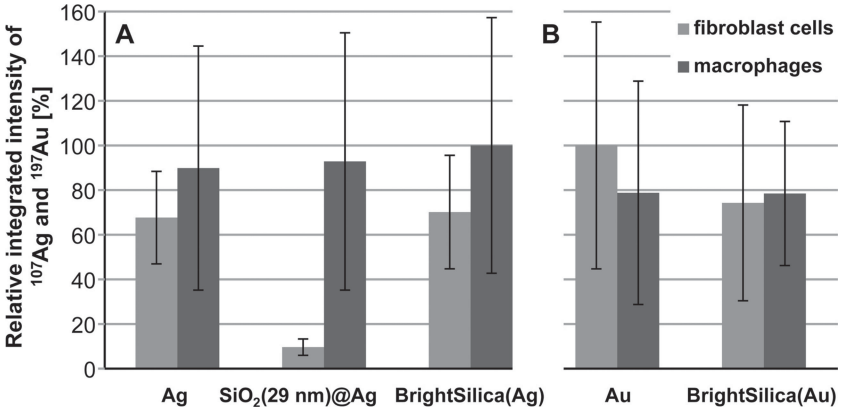

Figure 5. Relative integrated intensity of $^{107}Ag^+$ (A) and $^{197}Au^+$ (B) of single 3T3 fibroblast cells (green bars) and J774 macrophages (blue bars) exposed to uncoated silver and gold nanoparticles, BrightSilica(Ag), Bright Silica(Au), and SiO_2(29 nm)@Ag based on LA-ICP-MS data (see also Figures 4 and S8). Cells were exposed to nanoparticles for 24 h. The relative integrated intensity is given as mean value of 9–15 fibroblast cells and 25–30 macrophage cells, respectively, for each incubation condition. Standard deviation includes cell-to-cell variation regarding cell size, morphology and nanoparticle uptake. Parameters: Laser spot size 8 µm, scan speed 8 µm/s, repetition rate 5 Hz, fluence 0.6 J cm^{-2} (fibroblast cells) and 4.0 J cm^{-2} (macrophages).

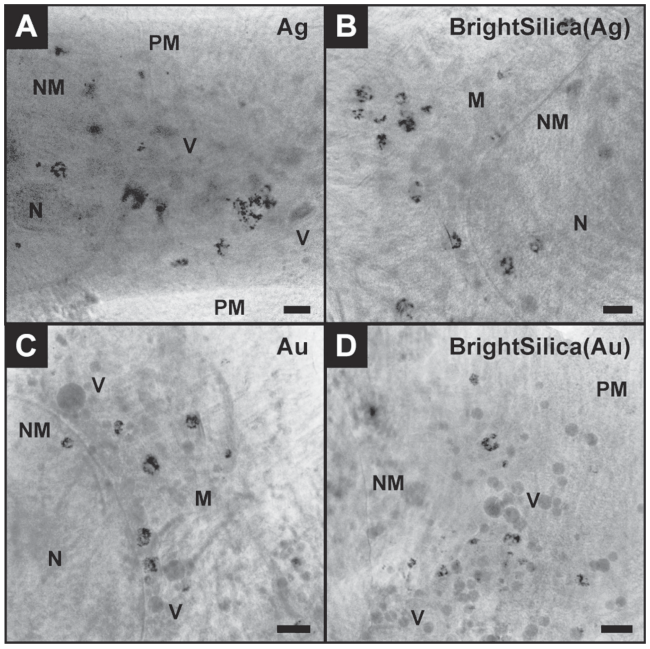

Figure 6. Nanoscale X-ray microscopic images of vitrified 3T3 fibroblast cells after incubation with (A) uncoated silver nanoparticles, (B) BrightSilica(Ag), (C) uncoated gold nanoparticles and (D) BrightSilica(Au). Cells were exposed to the nanoparticles in cell culture medium for 24 h. All images were acquired with a 25 nm zone plate (9.8 nm pixel size). Scale bars: 1 µm. Abbreviations: N, nucleus; NM, nuclear membrane; M, mitochondrion; V, vesicle; PM, plasma membrane.

aggregates differing in size and morphology are localized in phagosomes or endo-lysosomal vesicles in the cytoplasm. BrightSilica(Ag) shows a similar nanoparticle distribution in the cell architecture (Figure S10B) as uncoated silver nanoparticles (Figure S10A), while incubation of BrightSilica(Au) (Figure S10D) leads to bigger and more dense particle aggregates than BrightSilica(Ag). The differences in aggregate morphology can be attributed to different interactions of the particles among one another and with cellular components. In general, the arrangement of BrightSilica(Au) nanoparticles inside the macrophage cells is comparable with that of uncoated gold nanoparticles (Figure S10C), as was also discussed above for the fibroblast cells (Figure 6).

The Movie S3 of BrightSilica(Ag) does not provide evidence of ring-like nanoaggregates, unlike reported previously for citrate-stabilized silver nanoparticles.[10] Since a specific biomolecular corona of uncoated silver nanoparticles is probably associated with the formation of such structures,[10] the absence of nanorings further supports the hypothesis that the surface composition of BrightSilica(Ag) differs compared to silver nanoparticles.

2.5. SERS from Cellular Molecules Using the Plasmonic Cores of BrightSilica Nanoparticles

3T3 fibroblast cells and J774 macrophage cells incubated for 24 h with BrightSilica nanoparticles were studied in SERS mapping experiments. The experiments with BrightSilica yielded signal-rich SERS spectra both in fibroblast cells and in macrophages (**Figure 7**A,B). For comparison, identical experiments were conducted with uncoated gold nanoparticles in both cell lines (Figure 7C,D). The inclusion of the nanoparticles in discrete endosomal structures indicated in the X-ray microscopic data (Figure 6 and Figure S10) leads to a distribution of spectra with SERS signals over each respective mapped area, so that SERS spectra are obtained only from locations in the cells where BrightSilica nanoparticles are present. As a consequence, each set of data from a cell contains spectra with and without SERS signals. In macrophages, the number of SERS spectra per cell is very similar for uncoated gold and BrightSilica nanoparticles (~55 spectra per cell, almost all spectra). In the fibroblast cells the amount of spectra per cell with a SERS signature is ~60% of that obtained after the delivery of uncoated gold nanoparticles. Assuming similar behavior with respect to accumulation in the endosomes, as is suggested by X-ray microscopic images (Figure 6C,D), the results of this comparison are in good accordance with those obtained by LA-ICP-MS (Figure 5B) and are a further indicator of the smaller amount of BrightSilica than uncoated gold nanoparticles in the cells. BrightSilica, similar to uncoated gold nanoparticles,[9] forms intraendosomal aggregates (Figure 6 and Figure S10) that enable SERS signals of high intensities. As also illustrated in Figure S2A, aggregates of the BrightSilica nanoparticles possess a broad, extended plasmon band in the near-infrared, supporting the fact that excitation of the SERS with a wavelength of 785 nm is very efficient.

Figure 7 shows the full range of representative spectra extracted from the data sets of different cells. Band assignments are provided in Supporting Table S1. In accord with our previous findings with uncoated gold nanoparticles in epithelial cells,[9] the qualitative variations between the spectra are quite large, pointing at the heterogeneous environment in the endosomal and lysosomal structures. However, in all data sets obtained with BrightSilica nanoparticles, the amount of spectra that contain one common set of several bands ranges from 60–70%, with highest spectral uniformity observed in the macrophage cells (see also examples Figure 7B). Even though precise position and width of the bands in SERS spectra are usually slightly different from those in normal Raman spectra, it is possible to assign many bands, and in many cases there are sets of bands occurring at very similar intensity ratios. Most spectra have one set of at least six bands in common that can be assigned to amino acids, likely incorporated in a protein or peptide structure (Table S1). Specifically, they contain a band around 500 cm^{-1} that is also observed in the Raman spectra of amino acid mixtures at low pH,[23] a band around 630 cm^{-1} that can be assigned to the C-S stretching vibration of cysteine[24] or also to the side chain of tyrosine[23] (~650 cm^{-1}). Strong contributions of tyrosine become evident in the spectra of the macrophage cells, where a very uniform pattern attributed to the tyrosine side chain is found (Figure 7B), dominated by the ring breathing (~415 cm^{-1}) of Tyr, the Fermi resonance of its overtone with the symmetric ring-breathing (~830/850 cm^{-1}), and the C–C stretching vibration (~1130 cm^{-1}).[23] Furthermore, most spectra display a band at ~1009 cm^{-1} assigned to the aromatic ring vibration of phenylalanine.[25] The bands assigned to the amide III vibrations[23] of the peptide bond around 1300 cm^{-1} suggest that the amino acids are incorporated in proteins or peptides.

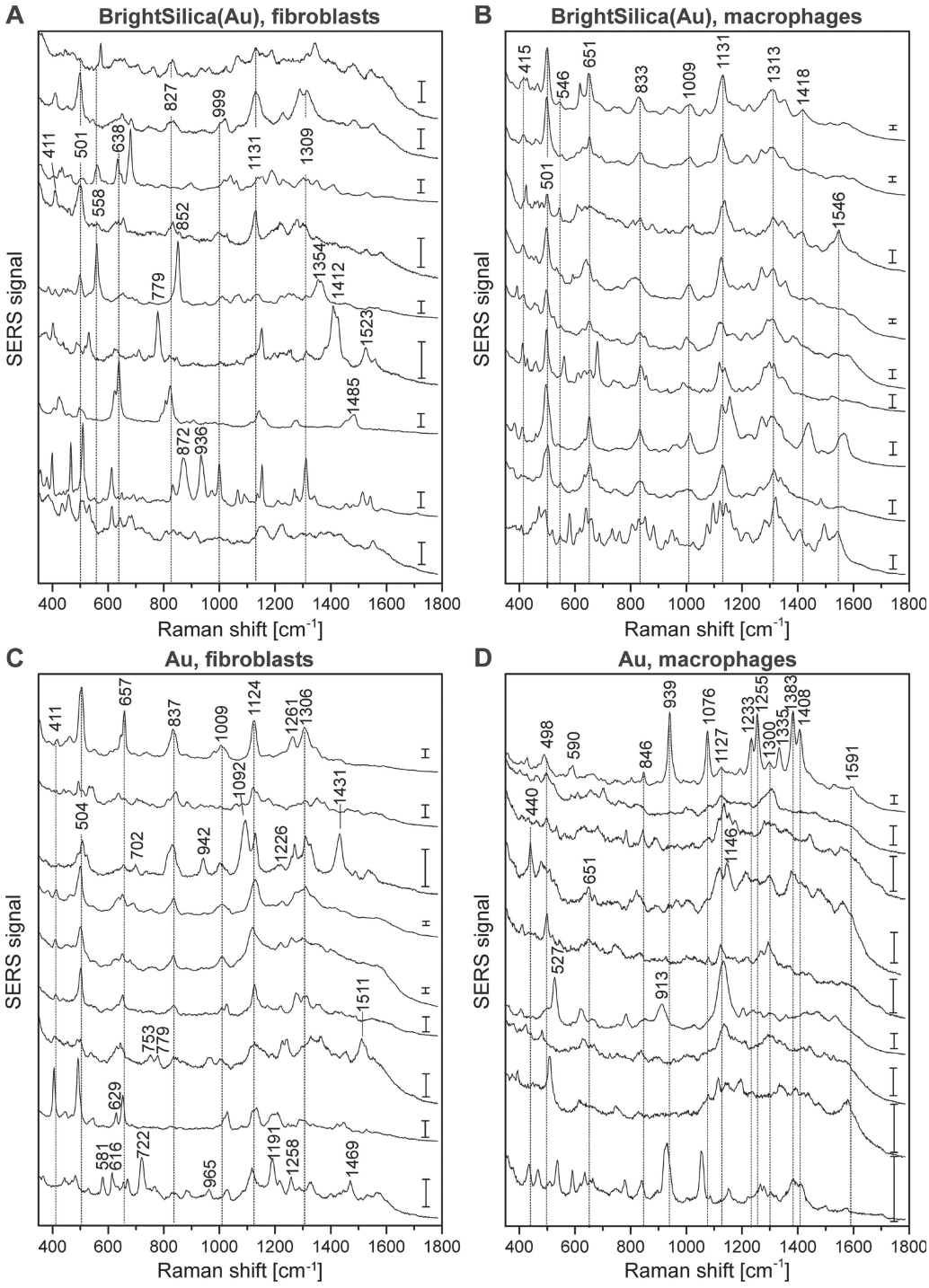

Figure 7. SERS spectra of 3T3 fibroblast cells (A,C) and J774 macrophages (B,D) exposed to BrightSilica(Au) (A,B) and gold nanoparticles (C,D), respectively, for 24 h. Three representative spectra of three individual cells are shown for each incubation condition. Band assignments are given in Supporting Table S1. Scale bars: 1000 cps. Excitation wavelength: 785 nm, accumulation time: 1 s, intensity: 1.9×10^5 W cm^{-2}.

The spectral signatures found for the same BrightSilica nanoparticles in the 3T3 fibroblast cells (Figure 7A) are less homogeneous than those in the macrophage cells. This confirms our previous observations of a different composition and/or variation of the molecular environment in the endosomes in different cell lines, leading to other interactions at the nanoparticle surface. Similar to the assignments in the fibroblast cells the spectra are dominated by bands of amino acid side chain vibrations (Table S1), even though the typical pattern assigned to tyrosine is found less frequently (Figure 7A).

The thickness of the silica shell of less than 2 nm can be held responsible for an electromagnetic SERS enhancement

occurring for molecules directly on the silica shell surface,[26] very similar to effects also observed for fluorescence enhancement.[27] However, in the case of the BrightSilica, the porosity of the silica will also enable a direct interaction of molecules with the plasmonic core. Integration into the silica is possible not only for small molecules,[28] but also for high-molecular weight compounds such as enzymes[29] and drugs in therapeutical approaches,[1a] also in combination with optical detection of multifunctional structures. The experiments with BrightSilica(Ag) nanoparticles in cells result in spectra that are basically invariant (Figure S11A,B; Table S1) and resemble those obtained with uncoated silver nanoparticles[10] in both cell lines (Figure S11C,D; Table S1). We have shown recently that the surface molecules of silver nanoparticles in cells are those the nanoparticles have interacted with in the cell culture medium, and that surface composition does not change due to strong adsorption to the silver surface,[10] a property that renders silver nanostructures very useful for protein detection by SERS,[30] and that is probably also governed by the concentration of protein/amino acid adsorbate.[31] From the spectra in Figure S11A,B we conclude that biomolecules in the cell culture medium interact with the silica and then remain associated with the silver core. Similar to uncoated silver nanoparticles not being suitable as SERS probes for this reason,[10] BrightSilica(Ag) is of limited use for investigations of silica nano-bio interaction. In contrast, the gold core does not bind the molecules that interact with the silica surface as strongly, and hence can retain availability for SERS of molecules at the silica surface inside the cell.

The SERS signals from the cells after incubation with BrightSilica can be used for SERS chemical imaging of the nanoparticles' surface composition and their optical localization inside the cells. Examples of chemical maps obtained with BrightSilica(Au) and BrightSilica(Ag) are displayed in **Figure 8**. In the case of BrightSilica(Au) (Figure 8B,D), the relative intensity of the tyrosine Raman signal at 1130 cm^{-1} (ν(C-C)) is shown as a function of the lateral coordinate. As this signal was observed in most of the spectra, the maps indicate the distribution of endosomes containing nanoparticles. To image the distribution of BrightSilica(Ag), the intensity of the cysteine band at 665 cm^{-1} (ν(C-S)) is shown (Figure 8F,H). In all maps, the perinuclear regions comprise high-intensity pixels, indicating that most nanoparticles accumulate around the nucleus, in accord with the X-ray microscopic observations of the nucleus, showing that particles are exclusively localized in the cytoplasm of the cells.

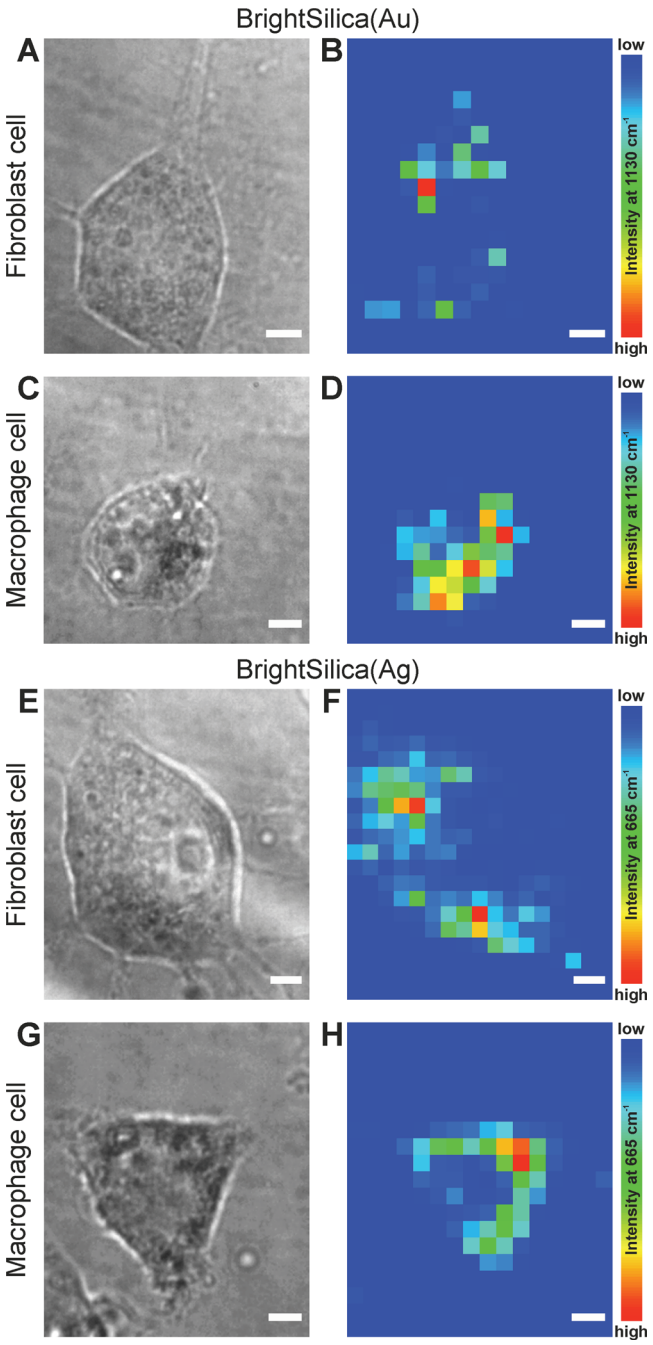

Figure 8. SERS chemical maps and corresponding bright field images of 3T3 fibroblast cells (A,B,E,F) and J774 macrophages (C,D,G,H) incubated with BrightSilica(Au) (A–D) and BrightSilica(Ag) nanoparticles (E–H) for 24 h. The relative intensity of the SERS signal at 1130 cm^{-1} (ν(C–C) of tyrosine) (B,D) and the band at 665 cm^{-1} (ν(C–S) of cysteine) (F, H), respectively, are displayed. Maps of cells exposed to uncoated gold and silver nanoparticles are shown in the Supporting Information for comparison (see Figure S12). Scale bars: 4 µm. Excitation wavelength: 785 nm, accumulation time per spectrum: 1 s, intensity: 1.9×10^5 W cm^{-2}, step width: 2 µm.

3. Conclusion

In order to investigate the interaction of silica nanoparticles with cultured eukaryotic cells, silica nanoparticles with a plasmonic core (BrightSilica) were used. The interaction of these silica-like nanostructures with biomolecules and the cellular environment was investigated with three complimentary methods employing the beneficial properties of the plasmonic metal core. Specifically, *i)* the local field around the gold core was used to observe the molecules interacting with the silica surface and sub-surface by their SERS spectra, *ii)* the high contrast in X-ray microscopic experiments allowed the reconstruction of tomograms and extraction of 3D information about their distribution in the cellular ultrastructure, and *iii)*

Table 1. Overview of the different particle types and main results of the SERS, X-ray microscopy and LA-ICP-MS studies. Abbreviations: t_{shell}, average thickness of the silica layer; d_{NP}, average particle diameter; σ, standard deviation of the mean values; *p*ATP, *para*-aminothiophenol.

	Particle size/shell thickness		SERS spectral information	X-ray microscopy: Particle localization		LA-ICP-MS: Relative amount of particles	
Particle type	$t_{shell} \pm \sigma$ [nm]	$d_{NP} \pm \sigma$ [nm]	3T3 / J774 cells	3T3 cells	J774 cells	3T3 cells [%]	J774 cells [%]
Au		31 ± 4	intracellular biomolecules	small aggregates in endosomes	small/large aggregates in endosomes/ phagosomes	100	79
BrightSilica(Au)	1.4 ± 0.3	31 ± 5				74	78
Ag		45 ± 20	components of cell culture medium	small aggregates in endosomes	small/large aggregates in endosomes/ phagosomes	68	90
BrightSilica(Ag)	1.7 ± 0.5	57 ± 20				70	100
SiO_2(29 nm)@Ag	29 ± 5	126 ± 26	*p*ATP reporter signature only	single particles and aggregates in endosomes	single particles and aggregates in endosomes/ phagosomes	10	93
SiO_2(49 nm)@Ag	49 ± 4	138 ± 25					

quantitative comparison of uptake of BrightSilica with uncoated nanoparticles was possible in LA-ICP-MS micromapping. The major results with regard to the silica nano-biointeraction are summarized in **Table 1**.

While the SERS enhancement factors of the non-aggregated BrightSilica nanoparticles are in agreement with those obtained for uncoated individual nanoparticles, inside the endosomes, where the BrightSilica nanoparticles aggregate, the homogeneous silica layer enables the coupling of the localized surface plasmons of the metal cores. The spectra reveal the presence of proteins at the surface of the BrightSilica nanoparticles, with the main contacts at the nano-bio interface formed by interaction via the side chains of tyrosine, cysteine, and phenylalanine. The comparison of the spectra obtained with BrightSilica(Au) in the macrophage cells and in the fibroblast cell line, suggests a different composition of the nanoparticle corona in the two cell types. Biomolecules, as extracellular molecules e.g., from culture medium are shown to penetrate into the thin silica layer of BrightSilica(Ag) and irreversibly bind to the silver surface. Thus, BrightSilica(Ag) is less suitable for in situ studies than BrightSilica(Au), which has implications for the further design of other 'Bright' nanoparticles, and also for systems that use silica-coated plasmonic nanostructures as SERS sensors.

The absorption of soft X-rays by the silica material gives sufficient contrast to visualize not only the plasmonic cores but also the silica shells in the cellular environment. Using cryo nanoscale X-ray tomography, we confirm the assumption that BrightSilica nanoparticles enter cells by an endocytotic mechanism that was observed before for pure silica nanoparticles.[4c,32]

Spatially resolved LA-ICP-MS showed that the uptake of BrightSilica nanoparticles with a gold core into fibroblast cells is slightly smaller than of uncoated gold nanoparticles of almost the same size, indicating a different interaction of the silica nanoparticles.

We have shown that the molecular interactions at the nano-bio interface of silica nanoparticles can be characterized by SERS, employing silica nanoparticles with plasmonic cores. The metal core enables precise 3D ultrastructural investigations and a reliable quantitative comparison regarding uptake rates and accumulation behavior for different nanomaterials. In general, the concept of 'Bright' nanoparticles enables multi-modal qualitative and quantitative characterization in comparative nanotoxicology and related fields of research.

4. Experimental Section

Gold and Silver Nanoparticle Synthesis: For metal nanoparticle preparation silver nitrate (99.9999%), tetrachloroauric(III)acid (99.9%), hydroxylamine hydrochloride and sodium hydroxide were purchased from Sigma-Aldrich Chemie GmbH (Germany) and tri-sodium citrate dihydrate (99%) from Merck (Germany). Millipore water (0.055 µS/cm; Purelab Plus, USF Elga Ultrapure) and ethanol were used as solvents. Silver nanoparticles were synthesized by reduction of silver nitrate with hydroxylamine hydrochloride according to a protocol described previously.[33] For the reduction of tetrachloroauric(III)acid tri-sodium citrate dihydrate was utilzed.[34]

Synthesis of Silica-Coated Nanostructures: All chemicals were purchased from Sigma-Aldrich Chemie GmbH (Germany) unless indicated otherwise. For the coating of the metal nanoparticle surface with silica shells of different thicknesses two different strategies were adapted:[35]

i. To obtain silver nanoparticles with thick silica shells (for comparison with the BrightSilica nanoparticles) and encapsulated reporter molecules, 5 mL of the nanoparticle suspension was added to a 90% ethanolic solution under stirring. After stirring for 15 min, 375 µL of 2×10^{-5} M (7.5 nmol) *para*-aminothiophenol (*p*ATP, 97%) were added. After the addition of 150 µL of 2 mM (0.3 µmol) ethanolic 3-aminopropyltriethoxysilane (APTES, 98%, ABCR GmbH & Co. KG, Germany), the suspension was mixed with 5 ml of 50 mM (250 µmol) ethanolic tetraethylorthosilicate (TEOS, ≥ 99%). The suspension was stirred for 15 min after each step. To initiate the aqueous reaction, 25 µL of 1 M sodium hydroxide (25 µmol) was added. The reaction mixture was stirred for 3 h under exclusion of light according to a modified protocol described in the literature.[36]
ii. BrightSilica nanoparticles were synthesized using a modified protocol adapted from work described in the literature.[35b] Briefly, for the activation of 10 mL of an aqueous sodium silicate solution with 0.54% SiO_2 (pure sodium silicate: Na_2O 10.6%, 26.5% SiO_2), 350 mg of the cation exchange resin Amberlite IRC86 (cation exchange resin, hydrogen form) were added, and the pH adjusted to pH 10. After the addition of 50 µL of 1 mM (50 nmol) aqueous solution of 3-aminopropyltrimethoxysilane (APTMS, 97%) to 10 mL of the nanoparticle

suspension, the mixture was stirred for 15 min. Then the suspension was mixed with 800 µL of the activated sodium silicate solution, and the pH was adjusted to pH 8 with 2.5% ammonium hydroxide solution. The reaction mixture containing gold nanoparticles was stirred for 3 h at 90 °C under exclusion of light.[37] For the synthesis of silica-coated silver nanoparticles, the reaction mixture was stirred for 48 h at room temperature under exclusion of light. Finally, the silica-coated nanoparticles were purified by centrifugation at 4000 rpm (~2000 g) for 15 min (Eppendorf 5430, Germany). After the second centrifugation step, particles were suspended in 1 mL ultrapure water.

Characterization of Silica-Coated Nanostructures: Particles were characterized by transmission electron microscopy (TEM) and energy-dispersive X-ray spectroscopy (EDX) using a Tecnai G^2 20 S-TWIN microscope (FEI, USA) with an acceleration voltage of 200 kV and a point resolution of 0.24 nm. Energy-filtered TEM (EF-TEM), electron energy loss spectroscopy (EELS) and scanning TEM (STEM) were performed with a JEOL JEM-200FS field emission transmission electron microscope (JEOL GmbH, Germany) with an acceleration voltage of 200 kV and a point resolution of 0.13 nm. Copper grids with a carbon-hole film (Formvar) were used for sample preparation.

Extinction spectra were recorded with a UV-Vis/NIR double-beam spectrophotometer (JASCO GmbH, Germany).

The stability of core–shell nanoparticles in cell culture medium was analyzed by dynamic light scattering using a Zetasizer Nano ZS (Malvern Instruments, United Kingdom) operating at a wavelength of 633 nm and a laser power of 4 mW at an angle of 173°. Intensity-weighted particle size distributions of three measurements are used for the determination of the hydrodynamic diameter.

Cell Culture: Mouse fibroblast cells (cell line 3T3) and macrophages (cell line J774; both from DSMZ, Germany) were cultivated in DMEM supplemented with 10% fetal calf serum (FCS) and 1% ZellShield (all from Biochrom AG, Germany) in a humidified environment at 37 °C and 5% CO_2. For the various experiments, cells were harvested and grown in sterile culture plates on the respective substrate (cover slips, coated X-ray grids). Under standard cell culture conditions, fibroblast cells and macrophages were incubated with uncoated and silica-coated gold and silver nanoparticles suspended in DMEM with 10% FCS. For all cell experiments, the same particle concentration was adjusted based on UV-Vis extinction. After an incubation time of 24 h, cells were washed thoroughly with PBS and immediately analyzed (SERS) or fixed (LA-ICP-MS, X-ray microscopy) depending on the subsequent method of analysis.

Normal Raman and SERS: Raman and SERS experiments were conducted with a LabRam HR Raman spectrometer (HORIBA Jobin Yvon GmbH, Germany) equipped with a 60× water immersion objective. An excitation wavelength of 785 nm was used in all experiments with an intensity at the sample in the range between $1.9 \cdot 10^5$ W cm^{-2} and $2.9 \cdot 10^6$ W cm^{-2} and an acquisition time of 1 s. The spectral resolution was ~2 cm^{-1}.

Enhancement factors of the nanoparticles were determined by the use of crystal violet (J.T.Baker, USA) following the procedure described previously.[15a] For the SERS experiments on living cells, fibroblasts and macrophages were grown on sterile cover slips and raster-scanned in 2 µm steps in a pre-defined grid of data points in PBS buffer. The laser spot size was ~1.5 µm in diameter. A MatLab (The MathWorks, Inc., USA) script was used for data processing and analysis of all SERS spectra.

Cryo Nanoscale X-ray Tomography: Cryo-XT was performed at beamline U41-XM equipped with a cryostage at the electron storage ring BESSY II (Helmholtz-Zentrum Berlin für Materialien und Energie, Germany).[13,38] For the cell experiments, mouse fibroblast cells and macrophages were grown as monolayer on Formvar-coated gold grids (Gilder Grids, England) under standard cell culture conditions. The growth medium (DMEM supplemented with 10% FCS) was replaced by medium containing uncoated and silica-coated silver and gold nanoparticles. After an exposure time of 24 h X-ray tomography grids were washed three times with PBS buffer, blotted with filter paper and snap-frozen on a plunge freezer using liquid ethane.

Projection images of vitrified cells with a thickness of up to about 10 µm were recorded at a tilt angle of 0°. Tilt series were obtained from single cells at different tilt angles in increments of 1°. The exposure time was adjusted for each tilt angle ranging from 2 to 24 s. A zone plate objective (outermost zone width 25 nm) was used leading to a pixel size of 9.8 nm. After pre-processing by flat-field correction (average from 10 flat-field images obtained under the same experimental conditions) the projection images were normalized to correct for different beam current and longer exposure times at higher tilt angles.

Laser Ablation ICP-MS: For LA-ICP-MS analysis, cells were grown on sterile cover-slips (Thermo Fisher Scientific, USA) and incubated with nanoparticles for 24 h under standard cell culture conditions. Prior to LA-ICP-MS analysis, the cells were washed thoroughly with PBS buffer and fixed with 4% *para*-formaldehyde in PBS and dehydrated in a graded series of ethanol/water mixtures.

LA-ICP-MS measurements of the isotopes ^{107}Ag and ^{197}Au were performed with an NWR213 laser ablation system (ESI, USA) coupled to an ICP sector field mass spectrometer (Element XR, Thermo Fisher Scientific, Germany). Representative sections of fixed fibroblast cells and macrophages were continuously ablated by line scans. Origin 8.5 (Originlab Corporations, USA) was used to convert each raw data point to a single pixel. ImageJ software[39] was applied for data analysis. The relative integrated intensity is given as mean value of 9–15 fibroblast cells and 25–30 macrophage cells. Experimental details on working conditions of the LA-ICP-MS are given in Table S2/S3 in the Supporting Information.

Supporting Information

Supporting Information is available from the Wiley Online Library or from the author.

Acknowledgements

D. Drescher and I. Zeise contributed equally to this work. We thank S. Selve (ZELMI TU Berlin) and H. Kirmse (HU Berlin) for TEM support, M. Weller and R. Schneider (BAM Federal Institute for Materials Research and Testing) for providing access to the cell culture facility. Financial support from ERC Grant No. 259432 (D.D., J.K.) and Einstein Stiftung Berlin (I.Z., J.K.) is gratefully acknowledged. We thank HZB for the allocation of synchrotron radiation beamtime and S. Werner and K. Henzler for technical support at the X-ray microscope.

Received: December 10, 2013
Revised: January 31, 2014
Published online: March 20, 2014

[1] a) M. Vallet-Regí, F. Balas, D. Arcos, *Angew. Chem. Int. Ed.* **2007**, *46*, 7548–7558; b) A. M. Fales, H. Yuan, T. Vo-Dinh, *Mol. Pharm.* **2013**, *10*, 2291–2298.

[2] a) W. S. Lin, Y. W. Huang, X. D. Zhou, Y. F. Ma, *Toxicol. Appl. Pharmacol.* **2006**, *217*, 252–259; b) T. J. Brunner, P. Wick, P. Manser, P. Spohn, R. N. Grass, L. K. Limbach, A. Bruinink, W. J. Stark, *Environ. Sci. Technol.* **2006**, *40*, 4374–4381; c) J. S. Chang, K. L. B. Chang, D. F. Hwang, Z. L. Kong, *Environ. Sci. Technol.* **2007**, *41*, 2064–2068; d) B. T. Mossman, A. Churg, *Am. J. Respir. Crit. Care Med.* **1998**, *157*, 1666–1680.

[3] A. J. Paula, R. T. Araujo Júnior, D. S. T. Martinez, E. J. Paredes-Gamero, H. B. Nader, N. Durán, G. Z. Justo, O. L. Alves, *ACS Appl. Mater. Interfaces* **2013**, *5*, 8387–8393.

[4] a) X. L. Huang, X. Teng, D. Chen, F. Q. Tang, J. Q. He, *Biomaterials* **2010**, *31*, 438–448; b) D. Napierska, L. C. J. Thomassen, V. Rabolli, D. Lison, L. Gonzalez, M. Kirsch-Volders, J. A. Martens, P. H. Hoet,

Small **2009**, *5*, 846–853; c) D. Drescher, G. Orts-Gil, G. Laube, K. Natte, R. Veh, W. Österle, J. Kneipp, *Anal. Bioanal. Chem.* **2011**, *400*, 1367–1373.

[5] a) P. Rivera Gil, G. Oberdorster, A. Elder, V. Puntes, W. J. Parak, *ACS Nano* **2010**, *4*, 5527–5531; b) L. Kastl, D. Sasse, V. Wulf, R. Hartmann, J. Mircheski, C. Ranke, S. Carregal-Romero, J. A. Martínez-López, R. Fernández-Chacón, W. J. Parak, H.-P. Elsasser, P. Rivera Gil, *ACS Nano* **2013**, *7*, 6605–6618.

[6] a) A. Lesniak, F. Fenaroli, M. R. Monopoli, C. Aberg, K. A. Dawson, A. Salvati, *ACS Nano* **2012**, *6*, 5845–5857; b) N. P. Mortensen, G. B. Hurst, W. Wang, C. M. Foster, P. D. Nallathamby, S. T. Retterer, *Nanoscale* **2013**, *5*, 6372–6380.

[7] a) M. P. Monopoli, D. Walczyk, A. Campbell, G. Elia, I. Lynch, F. Baldelli Bombelli, K. A. Dawson, *J. Am. Chem. Soc.* **2011**, *133*, 2525–2534; b) S. Tenzer, D. Docter, S. Rosfa, A. Wlodarski, J. Kuharev, A. Rekik, S. K. Knauer, C. Bantz, T. Nawroth, C. Bier, J. Sirirattanapan, W. Mann, L. Treuel, R. Zellner, M. Maskos, H. Schild, R. H. Stauber, *ACS Nano* **2011**, *5*, 7155–7167.

[8] a) Z. Wang, H. Wu, C. Wang, S. Xu, Y. Cui, *J. Mater. Chem.* **2011**, *21*, 4307–4313; b) H. Yuan, A. M. Fales, C. G. Khoury, J. Liu, T. Vo-Dinh, *J. Raman Spectrosc.* **2013**, *44*, 234–239; c) Z. Wang, S. Zong, J. Yang, J. Li, Y. Cui, *Biosens. Bioelectron.* **2011**, *26*, 2883–2889; d) Y. Cui, X.-S. Zheng, B. Ren, R. Wang, J. Zhang, N.-S. Xia, Z.-Q. Tian, *Chem. Sci.* **2011**, *2*, 1463–1469; e) L. Rodriguez-Lorenzo, Z. Krpetic, S. Barbosa, R. A. Alvarez-Puebla, L. M. Liz-Marzán, I. A. Prior, M. Brust, *Integr. Biol.* **2011**, *3*, 922–926.

[9] J. Kneipp, H. Kneipp, M. McLaughlin, D. Brown, K. Kneipp, *Nano Lett.* **2006**, *6*, 2225–2231.

[10] D. Drescher, P. Guttmann, T. Büchner, S. Werner, G. Laube, A. Hornemann, B. Tarek, G. Schneider, J. Kneipp, *Nanoscale* **2013**, *5*, 9193–9198.

[11] D. Drescher, C. Giesen, H. Traub, U. Panne, J. Kneipp, N. Jakubowski, *Anal. Chem.* **2012**, *84*, 9684–9688.

[12] a) D. Weiß, G. Schneider, B. Niemann, P. Guttmann, D. Rudolph, G. Schmahl, *Ultramicroscopy* **2000**, *84*, 185–197; b) E. Hanssen, C. Knoechel, N. Klonis, N. Abu-Bakar, S. Deed, M. LeGros, C. Larabell, L. Tilley, *J. Struct. Biol.* **2011**, *173*, 161–168; c) A. Sakdinawat, D. Attwood, *Nat. Photonics* **2010**, *4*, 840–848.

[13] G. Schneider, P. Guttmann, S. Heim, S. Rehbein, F. Mueller, K. Nagashima, J. B. Heymann, W. G. Müller, J. G. McNally, *Nat. Methods* **2010**, *7*, 985–988.

[14] S. D. Conner, S. L. Schmid, *Nature* **2003**, *422*, 37–44.

[15] a) V. Joseph, A. Matschulat, J. Polte, S. Rolf, F. Emmerling, J. Kneipp, *J. Raman Spectrosc.* **2011**, *42*, 1736–1742; b) C. J. Orendorff, L. Gearheart, N. R. Jana, C. J. Murphy, *Phys. Chem. Chem. Phys.* **2006**, *8*, 165–170.

[16] D. S. Wang, M. Kerker, *Phys. Rev. B* **1981**, *24*, 1777.

[17] A. Matschulat, D. Drescher, J. Kneipp, *ACS Nano* **2010**, *4*, 3259–3269.

[18] a) S. Kapishnikov, A. Weiner, E. Shimoni, P. Guttmann, G. Schneider, N. Dahan-Pasternak, R. Dzikowski, L. Leiserowitz, M. Elbaum, *Proc. Natl. Acad. Sci. USA* **2012**, *109*, 11188–11193; b) W. G. Müller, J. B. Heymann, K. Nagashima, P. Guttmann, S. Werner, S. Rehbein, G. Schneider, J. G. McNally, *J. Struct. Biol.* **2012**, *177*, 179–192.

[19] a) M. Al-Rawi, S. Diabate, C. Weiss, *Arch. Toxicol.* **2011**, *85*, 813–826; b) J. Blechinger, A. T. Bauer, A. A. Torrano, C. Gorzelanny, C. Bräuchle, S. W. Schneider, *Small* **2013**, DOI: 10.1002/smll.201301004; c) S. Quignard, G. Mosser, M. Boissiere, T. Coradin, *Biomaterials* **2012**, *33*, 4431–4442; d) F. Lu, S. H. Wu, Y. Hung, C. Y. Mou, *Small* **2009**, *5*, 1408–1413.

[20] a) C. Brandenberger, C. Muhlfeld, Z. Ali, A. G. Lenz, O. Schmid, W. J. Parak, P. Gehr, B. Rothen-Rutishauser, *Small* **2010**, *6*, 1669–1678; b) B. D. Chithrani, A. A. Ghazani, W. C. W. Chan, *Nano Lett.* **2006**, *6*, 662–668; c) S. E. A. Gratton, P. A. Ropp, P. D. Pohlhaus, J. C. Luft, V. J. Madden, M. E. Napier, J. M. DeSimone, *Proc. Natl. Acad. Sci. USA* **2008**, *105*, 11613–11618; d) A. E. Nel, L. Madler, D. Velegol, T. Xia, E. M. V. Hoek, P. Somasundaran, F. Klaessig, V. Castranova, M. Thompson, *Nat. Mater.* **2009**, *8*, 543–557.

[21] K. O. Yu, C. M. Grabinski, A. M. Schrand, R. C. Murdock, W. Wang, B. H. Gu, J. J. Schlager, S. M. Hussain, *J. Nanopart. Res.* **2009**, *11*, 15–24.

[22] a) H. Herd, N. Daum, A. T. Jones, H. Huwer, H. Ghandehari, C. M. Lehr, *ACS Nano* **2013**, *7*, 1961–1973; b) M. J. D. Clift, B. Rothen-Rutishauser, D. M. Brown, R. Duffin, K. Donaldson, L. Proudfoot, K. Guy, V. Stone, *Toxicol. Appl. Pharmacol.* **2008**, *232*, 418–427; c) O. Lunov, T. Syrovets, C. Loos, J. Beil, M. Delecher, K. Tron, G. U. Nienhaus, A. Musyanovych, V. Mailander, K. Landfester, T. Simmet, *ACS Nano* **2011**, *5*, 1657–1669.

[23] F. S. Parker, *Applications of Infrared, Raman, and Resonance Raman Spectroscopy in Biochemistry*, Plenum Press, New York/London **1983**.

[24] G. Diaz Fleming, J. J. Finnerty, M. Campos-Vallette, F. Célis, A. E. Aliaga, C. Fredes, R. Koch, *J. Raman Spectrosc.* **2009**, *40*, 632–638.

[25] a) J. De Gelder, K. De Gussem, P. Vandenabeele, L. Moens, *J. Raman Spectrosc.* **2007**, *38*, 1133–1147; b) S. Stewart, P. M. Fredericks, *Spectrochim. Acta A* **1999**, *55*, 1641–1660.

[26] J.-F. Li, S.-B. Li, J. R. Anema, Z.-L. Yang, Y.-F. Huang, Y. Ding, Y.-F. Wu, X.-S. Zhou, D.-Y. Wu, B. Ren, Z.-L. Wang, Z.-Q. Tian, *Appl. Spectrosc.* **2011**, *65*, 620–626.

[27] A. R. Guerrero, R. F. Aroca, *Angew. Chem.-Int. Ed.* **2011**, *50*, 665–668.

[28] T. Ung, L. M. Liz-Marzán, P. Mulvaney, *Langmuir* **1998**, *14*, 3740–3748.

[29] T. K. Jain, I. Roy, T. K. De, A. Maitra, *J. Am. Chem. Soc.* **1998**, *120*, 11092–11095.

[30] L. Chen, X. Han, J. Yang, J. Zhou, W. Song, B. Zhao, W. Xu, Y. Ozaki, *J. Colloid Interface Sci.* **2011**, *360*, 482–487.

[31] E. López-Tobar, B. Hernández, M. Ghomi, S. Sanchez-Cortes, *J. Phys. Chem. C* **2013**, *117*, 1531–1537.

[32] a) Z. Q. Chu, Y. J. Huang, Q. Tao, Q. Li, *Nanoscale* **2011**, *3*, 3291–3299; b) M. Ekkapongpisit, A. Giovia, C. Follo, G. Caputo, C. Isidoro, *Int. J. Nanomedicine* **2012**, *7*, 4147–4158.

[33] N. Leopold, B. Lendl, *J. Phys. Chem. B* **2003**, *107*, 5723–5727.

[34] P. C. Lee, D. Meisel, *J. Phys. Chem. A* **1982**, *86*, 3391–3395.

[35] a) W. Stöber, A. Fink, E. Bohn, *J. Colloid Interface Sci.* **1968**, *26*, 62–69; b) L. M. Liz-Marzán, M. Giersig, P. Mulvaney, *Langmuir* **1996**, *12*, 4329–4335.

[36] Y. Kobayashi, H. Inose, T. Nakagawa, K. Gonda, M. Takeda, N. Ohuchi, A. Kasuya, *J. Colloid Interface Sci.* **2011**, *358*, 329–333.

[37] J. F. Li, Y. F. Huang, Y. Ding, Z. L. Yang, S. B. Li, X. S. Zhou, F. R. Fan, W. Zhang, Z. Y. Zhou, D. Y. Wu, B. Ren, Z. L. Wang, Z. Q. Tian, *Nature* **2010**, *464*, 392–395.

[38] G. Schneider, P. Guttmann, S. Rehbein, S. Werner, R. Follath, *J. Struct. Biol.* **2012**, *177*, 212–223.

[39] W. S. Rasband, *ImageJ*, US National Institutes of Health, Bethesda, Maryland, USA, **1997–2014**; http://imagej.nih.gov/ij/, accessed January, 2014.